Implications of Wound Healing on Subcutaneous Photovoltaic Energy Harvesting

Maximilien Tholl, Marc Spring, Simone de Brot, Daniela Casoni, Adrian Zurbuchen, Hildegard Tanner, and Andreas Haeberlin

***Abstract*—Objective: Cardiac pacemakers must be regularly replaced due to depleted batteries. A possible alternative is proposed by subcutaneous photovoltaic energy harvesting. The body's reaction to an implant can cause device encapsulation. Potential changes in spectral light transmission of skin can influence the performance of subcutaneous photovoltaic cells and has not yet been studied in large animal studies. Methods: Subcutaneous implants measuring changes in the light reaching the implant were developed. Three pigs received those implants and were analyzed for seven weeks. Spectral measurements with known irradiation were performed to identify possible changes in the transparency of the tissues above the implant during the wound healing process. A histological analysis at the end of the trial investigated the skin tissue above the subcutaneous photovoltaic implants. Results: The implants measured decreasing light intensity and shifts in the light's spectrum during the initial wound healing phase. In a later stage of tissue recovery, the implants measured a generally reduced light intensity compared to the healthy tissue after implantation. The spectral distribution of the measured light at the end of the trial was similar to the first measurements. The histological analysis showed subcutaneous granulation tissue formation for all devices. Conclusion: The varying reduction of light intensity reaching the implants means that safety margins must be sufficiently high to ensure the power. At the end of the wound healing process, the spectral distribution of the light reaching the implant is similar to healthy tissue. Significance: Optimizations of spectral sensitivity of photovoltaic cells are possible.**

***Index Terms*—Energy harvesting, in-vivo trial, medical implant, subdermal photovoltaic cell, spectral light transmission, wound healing.**

Manuscript received March 14, 2021; revised April 29, 2021; accepted May 29, 2021. Date of publication June 4, 2021; date of current version December 23, 2021. This work was supported by Velux Foundation under Project number 1051. *(Corresponding author: Andreas Haeberlin.)*

Maximilien Tholl, Marc Spring, and Adrian Zurbuchen are with the Cardiac Technology and Implantable Devices, sitem Center, University of Bern, Switzerland.

Hildegard Tanner is with the Department of Cardiology, Inselspital, Bern University Hospital, University of Bern, Switzerland.

Simone de Brot is with the COMPATH, Institute of Animal Pathology, University of Bern, Switzerland.

Daniela Casoni is with the Experimental Surgery Facility, Department for BioMedical Research, University of Bern, Switzerland.

Andreas Haeberlin is with the Department of Cardiology, Bern University Hospital, CH-3010 Bern, Switzerland, and also with the Cardiac Technology and Implantable Devices, Sitem Center, University of Bern, CH-3010 Bern, Switzerland (e-mail: andreas.haeberlin@insel.ch).

Digital Object Identifier 10.1109/TBME.2021.3086671

I. Introduction

THE use of active electronic implants such as cochlear [1], retinal [2] and cardiac implants increased in recent years. Other examples of electronic diagnostic devices are implantable cardiac loop recorders [3] or continuous glucose-monitoring systems [4]. Electronic devices in general need to be supplied by electric energy which is provided by an internal battery. The cardiac pacemaker is the most common active electronic implant [5]. It has an average power requirement of below 10 μW and an average lifetime of about 7 years [6]. However, the median survival time of patients requiring permanent cardiac pacing is 8.5 years [7]. This discrepancy contributes to a high replacement rate of 25 $\%$ for cardiac pacemakers [8].

Energy harvesting within the human body presents an alternative to primary batteries. There are multiple approaches to harvest energy from e.g. body movement or blood flow, but this study focuses on subcutaneous photovoltaic cells which use light to recharge the implant. The idea of using subcutaneous photovoltaic cells to recharge active electronic implants has been previously studied and discussed. The light transmission of human skin was extensively modelled using Monte Carlo simulations [9]. A meteorological data evaluation estimated the real life potential of subcutaneous photovoltaic harvesting [10]. Further research on a medical photovoltaic power supply [11], an energy autonomous photovoltaic powered CMOS sensor [12] and a photovoltaic harvester specialized on infrared radiation [13] showed promising results. Moreover, an $ex\text{-}vivo$ trial irradiated a photovoltaic module below a flap of porcine skin [14]. Acute $in\text{-}vivo$ trials with implanted photovoltaic modules in mice [15], [16] and pigs [17], [18] showed promising power outputs. The trials showed that subcutaneous photovoltaic modules at implantable size scales can generate between 2-10 $mWcm^{-2}$ under midday solar irradiation. UV radiation is the main cause of photovoltaic cell ageing [19]. The human skin strongly absorbs UV radiation and therefore further increases the photovoltaic cell's durability, a competitive advantage compared to other energy harvesting mechanisms, which often rely on moving parts [20].

The aim of this study was to evaluate the influence of the wound healing process after implantation on the light reaching the implant and the spectral distribution of that light. Wound healing leads to tissue remodelling, device encapsulation after the implantation and will influence the power output. So far, $in\ vivo$ trials in literature are limited to short term experiments

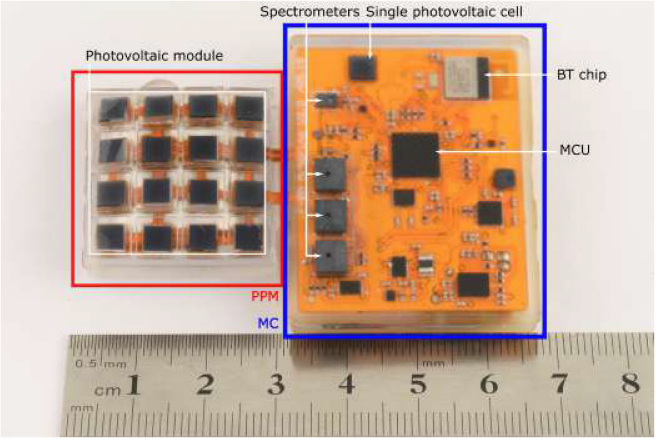

Fig. 1. The photovoltaic pacemaker measurement device as implanted in the animals. The photovoltaic pacemaker (PPM) is on the left, the measurement circuit (MC) part of the device is on the right. MCU = Microcontroller unit, BT = Bluetooth.

which do not consider wound healing after implantation. This long term *in vivo* trial during seven weeks provides new insights on the influence of wound healing for subcutaneous photovoltaic harvesting.

II. Methods

The potential of subcutaneous photovoltaic energy harvesting was tested in a long term *in vivo* trial. Subcutaneous photovoltaic pacemaker measurement devices were implanted into pigs. Subsequently, we describe the custom-made device, that was specifically built for this purpose and the experimental protocol of the long-term animal trial.

A. Photovoltaic Pacemaker Measurement Device

The implant, that was used in this trial, is a measurement device that enables to observe relevant changes within the skin tissue above the included subcutaneous photovoltaic module. It consists of two subsystems: a photovoltaic pacemaker (PPM) with a battery that is charged by a photovoltaic module and an independent measurement circuit (MC) with its own battery that supervises the PPM. The photovoltaic pacemaker is a fully functional cardiac pacemaker that constantly paces over a shunt resistance and is recharged by the photovoltaic cell array. The battery of the MC is charged by induction before the trial. The MC measures the PPM's current and voltage of the photovoltaic module and its battery voltage. Furthermore, it measures time, the open circuit voltage of a single photovoltaic cell, temperature, its own battery voltage and the spectrum of the light reaching the implant with 4 separate spectrometer ICs.

Fig. 1 shows the final prototype packaged in silicone (Elastosil RT 601 A/B [21], Wacker Chemie AG, Stuttgart, Germany). The photovoltaic module on the left, marked by the red box, consists of a 4 by 4 array of monocrystalline silicon photovoltaic cells (YKSM 4-4-0.5-5. [22], Yolk, Gyeonggi-do, Republic of Korea). The measurement circuit on the right, marked by the blue box, consists of many parts as e.g. the spectrometers, a single photovoltaic cell, a bluetooth (BT) chip for communication and a microcontroller unit (MCU) to handle all tasks. The single photovoltaic cell on the measurement circuit is equivalent to the cells on the photovoltaic module. It is unloaded and a good low-light indicator.

Prior to the animal trial, the devices were extensively tested on all functionalities as eg. performing measurements, communication via BT and many more. The photovoltaic cell array was able to keep the PPM's battery charged for indoor lighting conditions. Furthermore, the prototype remained submerged in water for six days and ethanol for one day.

1) Calibration of the Spectrometers on the Device: There are four spectrometer integrated circuits (ICs) on the device. Three (AMS AS7265x, 410 - 940 nm [23], ams International AG, Premstaetten, Austria) of them work together as one spectrometer system covering 18 channels. The last spectrometer (AMS AS7341, 410-670 nm [24], ams International AG, Premstaetten, Austria) works independently and provides 11 channels. The device's spectrometers were not calibrated. Therefore, a reference spectrometer (Ocean Optics USB 4000 [25], Ocean Optics Inc., Largo, Florida, USA) was used to measure the spectral irradiation of a 400 W halogen light source to calibrate the ICs in a spectral range of 500-850 nm. The prototype was placed next to the reference spectrometer's optical fiber. Both, the device to be calibrated and the optical fiber of the reference spectrometer, were placed in a box covered with a diffuser because the device's spectrometers are designed to be used for diffuse light only. The halogen lamp was placed orthogonally at one meter distance to the diffuser. The gain factors for each channel and for every spectrometer chip was adjusted to fit the reference spectrometer and to achieve maximum amplification without sensor saturation.

B. Animal Trial

The experiment received an ethical approval from Canton of Berne, Switzerland (Authorization number: BE87/19). The animals included in the trial were three juvenile 'Edelschwein' pigs (2-3 months old), 2 male and one female, weighing 29, 30 and 36 kg at the beginning of the trial. The porcine skin model was chosen because it is the most similar to humans in terms of cellular composition, anatomy and physiology [26].

1) Implantation: All devices were subcutaneously implanted on the pigs' flanks epifascially (as in conventional pacemaker implantations in humans). The surgical procedure was performed under general anaesthesia and consisted of a 6 cm long incision and tissue preparation and dissection until the muscle's fascia were reached. Subsequently, an epifascial pocket was formed and the device was inserted into it. After insertion, the pocket was closed by triple stitching. The implantations were performed in the Experimental Anaesthesia, Department of Veterinary Clinical Science, University Bern.

2) Reference Measurements: Reference measurements were performed regularly to investigate the open circuit voltage as well as the subcutaneous, spectral irradiation. During a reference measurement, a 400 W halogen lamp (Haloline Eco Superstar 64 702, Osram GmbH, Munich, Germany) was

positioned in a pre-calibrated 23 cm distance orthogonally above the skin covering the implant to act as a solar simulator. The measurements allow to observe changes in the spectral light distribution under the skin during the wound healing process. A reference measurement consists of a series of 30 fast, subsequent measurements, which are averaged and used for analysis of the above mentioned parameters.

All devices performed first reference measurements immediately after implantation. The last measurements were all performed with an identical device, which was placed in the subcutaneous pockets of the devices after their explantation. In contrary to the usual reference measurements, the first and last measurements were repeated for 100 cm distance to cross-check the measurement results and to reduce the influence of the correct light source distance. The correct measurement distance is very important as the light intensity in air decays proportionally to $1/distance^2$ [27].

3) First Week in the Veterinary Hospital: After implantation, the pigs were recovered from general anaesthesia under veterinarian care in single recovery boxes and transferred to the Swine and Ruminants Clinic of Department of Clinical Science, University Bern where close veterinarian supervision of their well-being was assured on a daily basis. Moreover, reference measurements with the above mentioned halogen lamp in 23 cm distance were performed once per day for every device.

4) Six Weeks At the Farm: After this phase the animals were transferred in group to a farm on the 6th or 7th post-operative day (POD). The farm offered a large stable (20 m^2) with constant water access and the animals were fed twice a day. They were kept in the stable for the first three days and then were allowed to access the 60 m^2 outside garden at any time. The reference measurements with the halogen lamp in 23 cm distance were repeated three times per week for the rest of the trial.

5) Explantation: After six weeks at the farm, the animals were transferred back to the Experimental Anaesthesia, Department of Veterinary Clinical Science, University Bern, to explant the devices under general anaesthesia. The first pig underwent euthanasia at the end of the experimental day. The two remaining pigs were recovered from general anaesthesia and were permanently transferred to a sanctuary farm. A skin sample over each device's spectrometers was extracted for histological analysis.

C. Histology

A histological analysis to identify relevant pathological changes and to determine the thickness of each skin layer (epidermis, dermis, subcutaneous tissue) and granulation tissue layer above the implant was performed. For this purpose, full thickness skin tissue samples of approximately 2 cm length and 5 mm width were extracted above the implant's spectrometers. They were then immediately fixed in 4% buffered formalin, trimmed and routinely processed and stained with hematoxylin and eosin for histological examination, which was performed by a board certified veterinary pathologist. Histology slides were digitized for taking measurements of the tissue layers using the software CaseViewer 2.4 (3DHistech Ltd.).

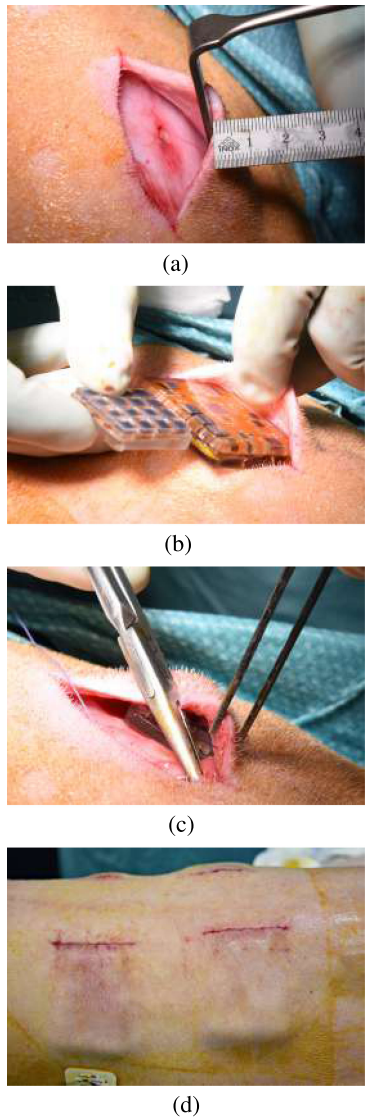

Fig. 2. Device implantation procedure at the beginning of the trial. (a) Preparation of the epifascial pocket for the device. (b) Insertion of the device into the epifascial pocket. (c) Stitching of the pocket.

III. Results

The following sections present the results that were acquired during and after the animal trial.

A. Animal Trial

The following subsections present the findings that were acquired during the animal trial.

1) Implantation: The implantation procedure was free from complications. The procedure and results of the implantation are illustrated in Fig. 2. No post-operative complications were detected.

2) Overview of Measurements: The implanted devices performed several measurements during the trial. Fig. 3 shows

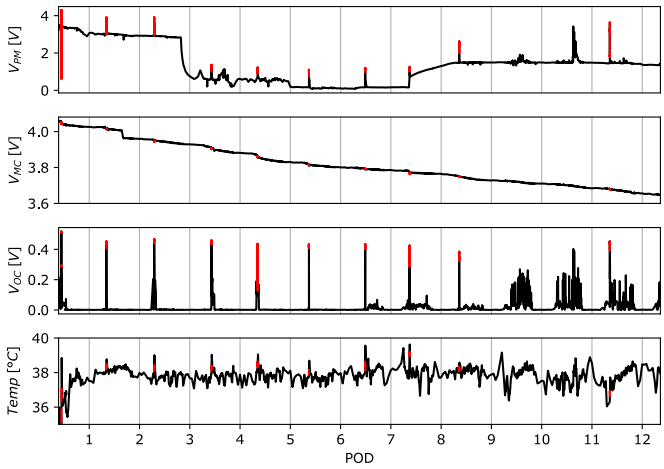

Fig. 3. Overview of exemplary measured parameters of one device. The figure shows the postoperative phase during the first two weeks. Data points of reference measurements under halogen lamp irradiation are marked in red. The pacemaker battery's voltage dropped on POD 2 which might indicate leakage currents and recovered on POD 7. The peaks in V_{OC} marked in red are due to an artificial light source used for reference measurements, the remaining peaks are caused by sunlight.

an exemplary overview of measured variables such as the voltage of the photovoltaic pacemaker battery V_{PM}, the voltage of the measurement circuit's battery (V_{MC}), the open circuit voltage of the single photovoltaic cell on the MC (V_{OC}) and the temperature ($Temp$) under the MC (facing the pig). The animals were transferred to the farm on POD 6 which lead to a visible increase of V_{OC} during daytimes. The V_{OC} is a good indicator for available light under low light conditions. The animals were allowed to leave the stable and stay on an open, mostly shaded field from POD 9 on, which led to a further significant increase of V_{OC} during daytime. The temperature stayed constant during the trial and did not indicate inflammatory responses or device malfunctions that led to heating of the device.

3) Power Output: The power output of the subdermal photovoltaic module dropped from 2.26 +/− 1.46 mW to 1.7 +/− 0.86 mW with the halogen lamp in 23 cm distance and an active area of 2.56 cm^2 when the first and last measurements are compared. This corresponds to a power density of 0.88 mW/cm^2 and 0.66 mW/cm^2 at the beginning and the end of the trial. The power of the halogen light source in 23 cm distance is approximately 100 mW/cm^2. The subcutaneous photovoltaic module was able to harvest 0.88 % of the irradiance's power at the beginning of the trial and 0.66 % at the end.

4) Open Circuit Voltage: The open circuit voltage V_{OC} of the single photovoltaic cell on the measurement circuit is an indicator of the available light within the sensitive spectrum (approximately 400 nm - 1000 nm) of the monocrystalline silicon photovoltaic cell in low light conditions.

First vs. last measurement. The measurements in 23 cm and 100 cm distance show that the open circuit voltage of the single photovoltaic cell decreased for all devices between the first and the last measurement (see Fig. 4). The mean ± SD V_{OC} across all devices dropped from 0.51 ± 0.02 V to 0.44 ± 0.04 V in 23 cm distance (p = 0.016, Wilcoxon signed-rank test). For 100 cm distance, the V_{OC} dropped from 0.32 ± 0.02 V to 0.23 ± 0.03 V (p = 0.016, Wilcoxon signed-rank test). This corresponds to a reduction of V_{OC} by 14.1% and 28.9% between the first and last measurement in 23 cm and 100 cm distance, respectively.

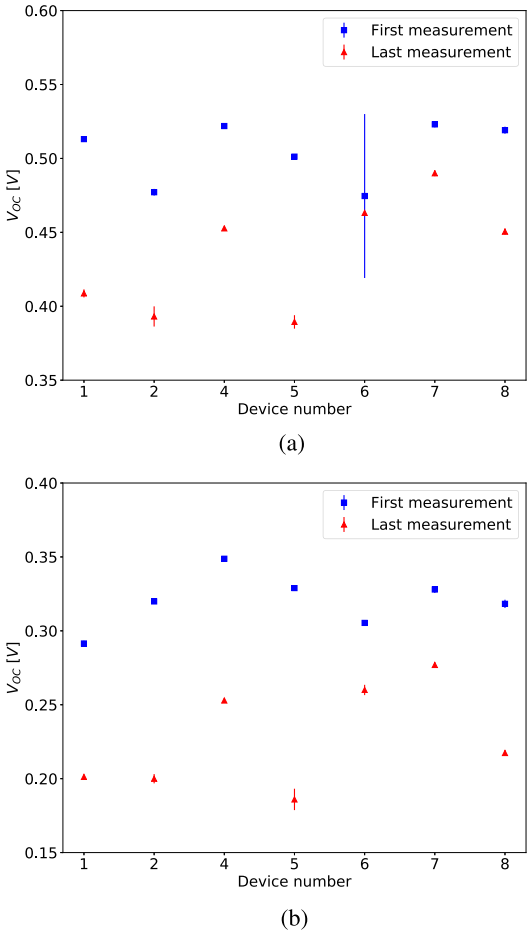

Fig. 4. Open circuit voltage (mean ± SD) of the single photovoltaic cell on the MC during reference measurements in different distances on the first and last day of the trial for all devices. (a) 23 cm distance. (b) 100 cm distance.

5) Spectral Light Measurements: The spectral distribution of light reaching the implant was measured during reference measurements with the halogen light source. The spectrometers are not calibrated for power measurements so only intensity shifts within the spectra can be detected. Non-calibrated data is plotted on grey background for all figures with spectral results.

First vs. last measurement. The absolute values of first spectrometer sensor (AS7265X) measured with the halogen lamp in 23 cm distance at the beginning and end of the animal trial are shown in the top panel of Fig. 5. The spectrum of the halogen lamp is plotted in black, illustrating the lamp's spectral radiation without skin coverage of the sensor. The mean spectral intensities during the first (blue) and last (red) measurement for all devices are presented in the top panel of Fig. 5. The mean spectral intensities for all devices show an approximately even reduction in intensity across all wavelengths. A comparison to the known spectral irradiation of the halogen light source shows that shorter wavelengths are increasingly absorbed by the skin

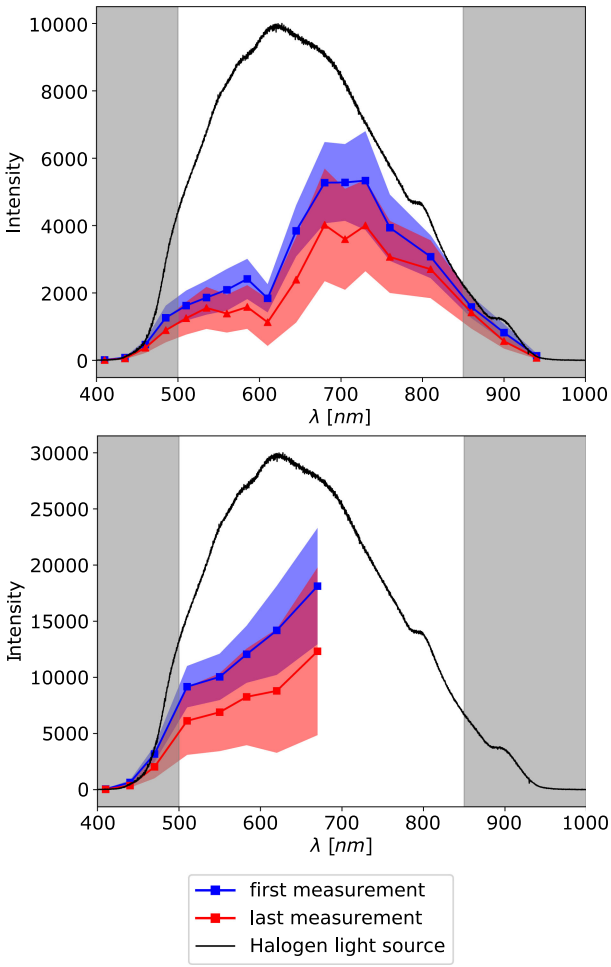

Fig. 5. Absolute values (mean ± SD of all Devices) of both spectrometer sensors during reference measurements with 23 cm distance on the first and last day of the trial. The top and bottom panels show results of the AMS AS7265X and the AMS AS7341 sensor, respectively. The solid lines represent mean values of the reference measurements and the shaded areas represent the respective standard deviations.

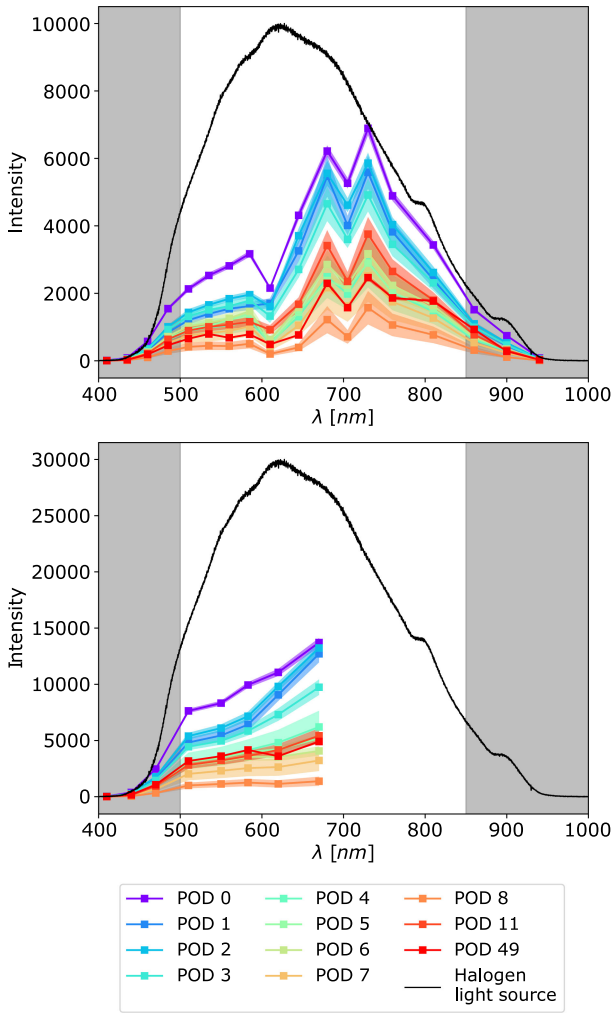

Fig. 6. Absolute values (mean ± SD) of the spectrometers during reference measurements for one device. The top and bottom panels show results of the AMS AS7265X and the AMS AS7341 sensor, respectively. The solid lines represent mean values of the reference measurements and the shaded areas represent the respective standard deviations.

tissue. There is an absorption peak at a wavelength of 610 nm. The bottom panel of Fig. 5 shows the absolute values of the second sensor (AS7341) measured with the halogen lamp in 23 cm distance at the beginning and end of the animal trial. The results of the second sensor support the findings of sensor 1 (AS7265X). On average, the intensities of all channels are reduced in an advanced wound healing phase.

Development over time. The measured spectral light distribution during reference measurements for one device are shown in Fig. 6. The black line shows the spectrum of the light source measured without obstruction in front of the sensor at an arbitrary amplitude for visualization purposes. The coloured solid lines show the mean values and the shaded areas the standard deviations of the individual reference measurements.

6) Explantation: The explantation procedure for the animal in the acute trial is shown in Fig. 7. The device visually did not appear to be damaged at first glance during explantation. A device encapsulation consisting of granulation tissue had formed around the implant. The inner surface of the encapsulation was smooth and did not grow into the device.

B. Histology

Fig. 8 shows two exemplary histological slides of the skin above the implant collected at the time of explantation. A summary of the measured skin layer thicknesses is given in Table I. A mean ± SD of the individual skin and granulation layers' thickness and the overall thickness was calculated from three measurements at different locations across the sample. Total skin thickness above the implants varied significantly between 8.9 and 17.9 mm. Epidermis and dermis showed lower absolute variations across the samples than other layers. Large thickness variations were observed in the subcutaneous fatty layer between 4.3 mm and 10.1 mm and in the granulation tissue layer from 1.5 mm to 5.6 mm.

The skin tissues revealed a variably thick layer of granulation tissue in the deep subcutaneous adipose tissue adjacent to the

TABLE I
MEAN AND STANDARD DEVIATION IN mm OF THREE THICKNESS MEASUREMENTS AT DIFFERENT LOCATIONS OF THE HISTOLOGICAL SKIN SAMPLES ABOVE THE INDICATED IMPLANTS

Skin layer	Thickness [mm]	Skin above device number: 1	2	3	4	5	6	7	8
All layers	mean	14.602	12.321	17.866	16.535	11.325	9.868	8.869	16.623
	SD	0.909	0.462	0.716	0.720	0.354	0.139	0.171	0.132
Epidermis	mean	0.172	0.218	0.171	0.168	0.168	0.201	0.149	0.181
	SD	0.060	0.012	0.020	0.065	0.042	0.085	0.010	0.029
Dermis	mean	2.797	2.366	2.990	2.231	2.484	2.354	2.372	2.295
	SD	0.223	0.343	0.071	0.177	0.368	0.148	0.199	0.502
Subcutaneous fatty layer	mean	8.280	8.173	10.060	8.085	4.877	5.681	4.344	8.009
	SD	0.468	0.750	0.246	0.419	0.407	0.157	0.536	0.399
Granulation tissue layer	mean	3.598	1.507	4.447	5.525	3.779	1.980	1.971	5.618
	SD	0.577	0.196	0.569	0.867	0.223	0.403	0.381	0.930

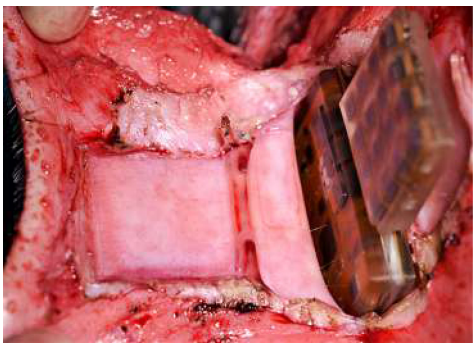

Fig. 7. Device 5 explantation procedure at the end of the trial.

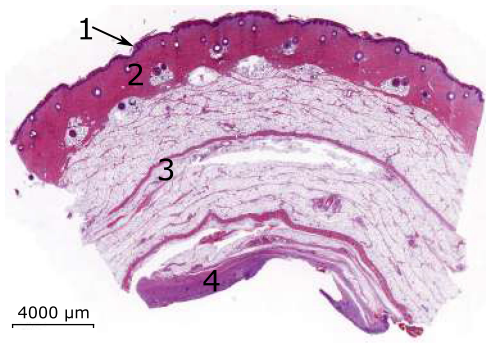

(a)

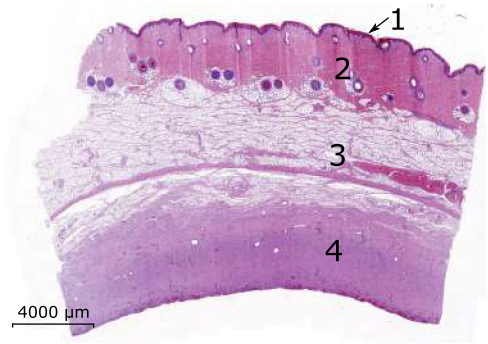

(b)

Fig. 8. Exemplary histological slides of the skin above the named devices. The epidermis (1) is a thin layer on top of the slide, the dermis (2) is a dense, vascularized tissue below the epidermis and the subcutaneous tissue (3) consists mainly of adipocytes. Note the variably thick layer of granulation tissue (4) in the deep subcutaneous tissue. The tissue slides were stained with hematoxylin and eosin. (a) Device 2. (b) Device 5.

implantation site in all assessable cases. Within the granulation tissue, a mild to moderate, multifocal hemorrhage was common and a mild to moderate, perivascular, predominantly lymphocytic and eosinophilic cellular inflammatory response was observed in all cases. In addition, two cases were characterized by the presence of foreign material (interpreted as silicone), accompanied by a mild granulomatous inflammatory response. The observed material is suspected to correspond to the devices silicone rubber packaging. This material is known to persist in tissues for a long time [28].

IV. DISCUSSION

The presented animal trial showed that the light intensity reaching the implant is reduced during the wound healing process due to a varying thickness of granulation tissue around the implant. Furthermore, partial shading of a subdermal implant can occur due to differences in granulation tissue thickness along the implant.

A. Animal Trial

This section discusses the results that were acquired during the animal trial. The power output of the PPM's photovoltaic module was not evaluated because all devices showed an accelerated battery drain. The low voltage of the PPM's battery meant that the energy harvesting IC 'BQ25570' [29] (Texas Instruments Incorporated, Dallas, Texas, USA) was not in its intended work mode. As a consequence, power measurements are only partially meaningful and cannot be interpreted reliably.

1) Open Circuit Voltage: The open circuit voltage of the single photovoltaic cell on the MC is a good indicator for the available subcutaneous light because it is very sensitive to changes in low light conditions. The maximum V_{OC} of the particular photovoltaic cell is 0.626 V which means that it was never saturated during the measurements and therefore provides reliable results. V_{OC} decreased for all devices between the first and last measurement.

2) Spectral Light Measurements: The spectral light intensities were measured by the two spectrometers on the MC to observe potential changes in the spectral distribution of light reaching the implant $in\ vivo$. The measurements

might allow to detect absorbers in certain spectral ranges during the wound healing process. However, the measurements do not allow to calculate spectral light transmission curves.

The comparison between the first and the last measurements showed that the light intensities decreased evenly for all wavelengths. The increased absorption of light for shorter wavelengths in the skin is in line with the results of our previously conducted Monte Carlo simulations [9] and can be expected because of the spectral absorption coefficient of the skin's constituents (melanosomes, blood, fat,...). An increased light absorption at 610 nm was observed by sensor AS7265X (Fig. 5, top panel) which is more pronounced at the beginning of the trial. It cannot be explained by an increased absorption coefficient of melanosome [30], blood [31], water [32] or fat [33]. Moreover, a local coverage of the sensor is very unlikely because the sensor IC is protected by the silicone rubber packaging and very close to other channels which would have been affected as well. Generally, the increased tissue thickness led to decreased light under the skin. However, the spectral distribution of light reaching the implant in the last measurement at an advanced wound healing stage did not substantially differ from the first measurement.

Observing the exemplary development of spectral measurements of one device (see Fig. 6) shows that the spectral distribution of the light reaching the implant is not evenly decreasing during the initial wound healing phase, as might be expected if only the first and last spectral measurements are compared. Both spectrometers measured a large decrease in intensities for wavelengths 500 - 600 nm during the first post-operative day. The absorption coefficient of blood exhibits a local peak in the same wavelength range [31]. The measured drop in intensities could therefore be explained by internal bleeding after implantation. Subsequently, the intensities of wavelengths 600-800 nm decrease faster than for the shorter wavelengths (500-600 nm). This could be explained by the general tissue growth and remodelling, vascularization and development of granulation tissue around the implant [34] leading to a broadband absorption that increases over time. The drop in intensities for shorter wavelengths could be decreased compared to wavelengths $>$ 600 nm because the tissue remodelling removes the highly absorbing internal bleeding and therefore counteracts the increasing general absorption. After 11 days, the intensities increased again. This might indicate that the acute wound healing with pronounced vascularization and possible inflammation ended and the tissue remodelling reached a state that is closer to the healthy tissue directly after implantation. The last measurement shows decreased intensities across all wavelengths except for $\lambda > 800\ nm$. The decrease of intensities can be explained by the significant growth of skin tissue above the implants during the full trial. The higher the wavelengths, the higher the penetration depth for light within the visible and near IR spectrum. This could explain that the intensities for $\lambda > 800\ nm$ did not decrease as much in the advanced wound healing phase.

In summary, our spectral light measurements suggest that the spectral distribution of light reaching the implant in an advanced wound healing phase reached a state that is not different to the spectral distribution of light under healthy tissue measured directly after implantation. However, during the acute wound healing phase in the first two weeks significant shifts in the spectral distribution of light reaching the implant were observed.

B. Histology

Granulation tissue, which consists of well vascularized connective tissue is known to form in response to skin implants [34]. The varying extent of granulation tissue in the examined skin samples may indicate a difference in the implant placement (implantation depth, relative positioning to ribs), mechanical loads or the individual foreign body response of the pigs.

The explanted tissue samples were fixed in formaldehyd without tension and therefore tend to bend and might appear thicker than in its stretched, natural state. Although this is true for all tissue samples, variations in e.g. sample length or width might lead to an altered bending and consequently thickness outcome. The true skin thicknesses $in\ vivo$ might be thinner than measured in the histological slices because the skin usually is under tension.

Tissue fixation and processing may cause an artefactual variation in tissue layer thickness. Microscopic thickness measurements may therefore be slightly imprecise and require interpretation with certain caution. The large variation of the total skin thickness reflect the differences in total body weight and growth of the animals during the trial. Moreover, the variations of thickness in subcutaneous fatty layer and granulation tissue layer show that the design of a subcutaneous photovoltaic implant needs to consider the worst case scenario and increase the safety margins for sufficient power generation.

The total skin thickness measurements show a rather low standard deviation within one sample. That means that the total tissue thickness above one implant is approximately constant. However, the fractions of the individual layers contributing to the total thickness are not constant (see Table I). The transparency across the layers varies and therefore the total skin thickness is not sufficient for a power output prediction.

The thicknesses of individual layers showed the highest relative standard deviations in the epidermis and the granulation tissue layer. The variation in thickness of the epidermis is considered physiological and less relevant because of its overall thinness. However, the larger standard deviation of the granulation tissue layer is important for the development of a subcutaneous photovoltaic module. The granulation tissue is dense, protein-rich and can be highly vascularized and therefore light absorbing. If that is the case and the thickness of granulation tissue varies significantly above the implant, partial 'shading' of the photovoltaic cell array can occur. This can significantly reduce the photovoltaic cell array's efficiency [35]. An overview over various different circuit and control techniques to optimize the efficiency of a photovoltaic cell arrays under partial shading were simulated and compared based on different requirements [36]. Further modelling of partially shaded photovoltaic cell arrays showed that a 'Total-Cross-Tied' assembly of the photovoltaic

cells performs best under partial shading conditions [37]. Granulation tissue is usually replaced by non-vascularized, collagenous scar tissue in the long-term [38] which should be less light absorbing than dermal tissue [39].

C. Illumination and Possible Applications

The power output of the subcutaneous photovoltaic module depends on the intensity and spectral distribution of the illumination. Solar radiation is one possible source for illumination that varies in intensity during the day. Furthermore, artificial light sources in buildings can contribute significantly to the harvested energy [40]. Partial irradiation due to shadows and covering of the skin above the implants by e.g. clothes can reduce the subcutaneous photovoltaic module's power output.

Subcutaneous photovoltaic harvesting could be envisioned as a power source for a wide range of biomedical implants such as glucose sensors or vital parameter monitors for example.

V. Conclusion

The results of the long-term porcine animal trial revealed important findings for subcutaneous photovoltaic energy harvesting. Generally, the available light (and therefore the power) below the skin will be reduced by different magnitudes depending on the total skin thickness and the level of granulation tissue formation that is part of the normal wound healing process and expected to occur as a reaction to skin implants. The granulation tissue can lead to partial shading of the subcutaneous photovoltaic array due to variations in thickness across one implant. The spectral distribution of light below the skin changes during the wound healing process but remains very similar compared to healthy tissue. In future studies, optimizations of the photovoltaic cell's spectral sensitivity for the subcutaneous light are possible.

Glossary

PPM	photovoltaic pacemaker
MC	measurement circuit
BT	bluetooth
PCB	printed circuit board
POD	post-operative day
V_{PM}	voltage of the photovoltaic pacemaker's battery $[V]$
V_{MC}	voltage of the measurement circuit's battery $[V]$
V_{SC}	voltage across the whole photovoltaic cell array on the photovoltaic pacemaker $[V]$
SD	standard deviation
V_{OC}	open circuit voltage $[V]$
$Temp$	temperature $[°C]$
λ	wavelength $[nm]$

Appendix A
Photovoltaic Pacemaker Measurement Device - Technical Descriptione

A. Photovoltaic Pacemaker Measurement Device

The implant, that was used in this trial, is a measurement device that enables to observe relevant changes within the skin tissue above the included subcutaneous photovoltaic module. It consists of two main subsystems: a photovoltaic pacemaker (PPM) with a battery that is charged by a photovoltaic module and an independent measurement circuit (MC) with its own battery that supervises the PPM. The photovoltaic pacemaker is a fully functional cardiac pacemaker that constantly paces over a shunt resistance and is recharged by the photovoltaic cell array. The battery of the MC is charged by induction before the trial. The MC measures the PPM's current and voltage of the photovoltaic module and its battery voltage. Furthermore, it measures time, the open circuit voltage of a single photovoltaic cell, temperature, its own battery voltage and the spectrum of the light reaching the implant with 4 separate spectrometer ICs.

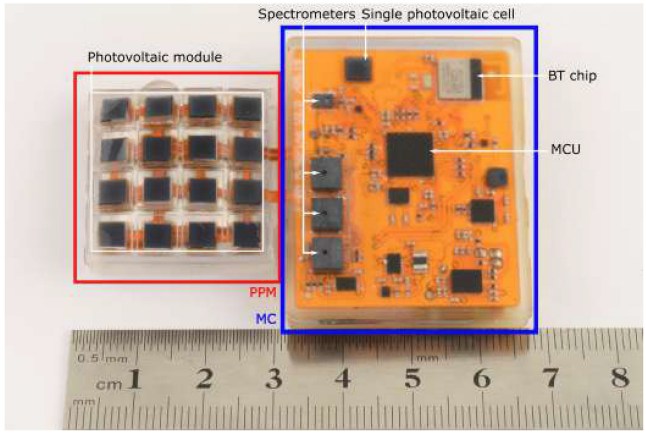

Fig. 9. The photovoltaic pacemaker measurement device as implanted in the animals. The measurement circuit part of the device is on the right, the photovoltaic pacemaker is on the left.

Fig. 9 shows the final prototype packaged in silicone rubber (Elastosil RT 601 A/B [21], Wacker Chemie AG, 70 191 Stuttgart, Germany). The photovoltaic module on the left, marked by the red box, consists of a 4 by 4 array of monocrystalline silicon photovoltaic cells (YKSM 4-4-0.5-5. [22], Yolk, Gyeonggi-do, Republic of Korea). The cells are connected with 4 times 4 cells in series, which were then connected in parallel. The measurement circuit on the right, marked by the blue box, consists of many parts as e.g. the spectrometers, a single photovoltaic cell, a bluetooth (BT) chip for communication and a microcontroller unit (MCU) to handle all tasks. The single photovoltaic cell on the measurement circuit is equivalent to the cells on the photovoltaic module.

Prior to the animal trial, the devices were extensively tested on all functionalities as eg. performing measurements, communication via BT and many more. The photovoltaic cell array was able to keep the PPM's battery charged for indoor lighting conditions. Furthermore, the prototype submerged in water for six days and ethanol for one day.

1) Calibration of the Spectrometers on the Device: There are four spectrometer ICs on the device. Three (AMS AS7265x, 410 - 940 nm [23], ams International AG, 8141 Premstaetten, Austria) of them work together as one spectrometer system covering 18 channels. The last spectrometer (AMS AS7341, 410-670 nm [24], ams International AG, 8141 Premstaetten,

Austria) works independently and provides 11 channels. The device's spectrometers were not factory calibrated. Therefore, a reference spectrometer (Ocean Optics USB 4000 [25], Ocean Optics Inc., 33 777 Largo, Florida, USA) was used to measure the spectral irradiation of a 400 W halogen light source. The prototype was placed next to the reference spectrometer's optical fiber. Both, the device to be calibrated and the optical fiber of the reference spectrometer, were placed in a box covered with a diffuser because the device's spectrometers are designed to be used for diffuse light only. The halogen lamp was placed orthogonally in one meter distance to the diffuser. The gain factors for each channel and for every spectrometer chip was adjusted to fit the reference spectrometer and to achieve maximum amplification without sensor saturation. The signal amplitude of the halogen light source on the reference spectrometer is low for $\lambda < 500$ nm and $\lambda > 850\,nm$. Therefore, a reliable calibration is possible only for wavelengths 500 - 850 nm.

Acknowledgment

The authors thank Act-Inno AG for the access to their testing facilities. Declarations of interest: None relevant to this work.

References

[1] T. Lenarz, "Cochlear implant – state of the art," *GMS Current Top. Otorhinolaryngol. – Head Neck Surg.*, vol. 16, no. 4, 2017. doi:10.3205/CTO000143.

[2] J. O. Mills, A. Jalil, and P. E. Stanga, "Electronic retinal implants and artificial vision: Journey and present," *Eye*, vol. 31, pp. 1383–1398, May 2017.

[3] A. Bisignani *et al.*, "Implantable loop recorder in clinical practice," *J. Arrhythmia*, vol. 35, pp. 25–32, Nov. 2018.

[4] M. Gray *et al.*, "Implantable biosensors and their contribution to the future of precision medicine," *Vet. J.*, vol. 239, pp. 21–29, Sep. 2018.

[5] J. Bogaert *et al.*, *Clinical Cardiac MRI*. Berlin, Germany: Springer-Verlag, Feb. 2012, p. 58.

[6] D. Katz and T. Akiyama, "Pacemaker longevity: The worlds longest-lasting VVI pacemaker," *Ann. Noninvasive Electrocardiol.*, vol. 12, pp. 223–226, Jul. 2007.

[7] M. Brunner, "Long-term survival after pacemaker implantation prognostic importance of gender and baseline patient characteristics," *Eur. Heart J.*, vol. 25, pp. 88–95, Jan. 2004.

[8] H. Mond and A. Proclemer, "The 11th world survey of cardiac pacing and implantable cardioverter-defibrillators: Calendar year 2009-a world society of arrhythmias project," *Pacing Clin. Electrophysiol.*, vol. 34, pp. 1013–1027, Jun. 2011.

[9] M. Tholl *et al.*, "Subdermal solar energy harvesting a new way to power autonomous electric implants," *Appl. Energy*, vol. 269, Jul. 2020, Art. no. 114948.

[10] M. V. Tholl *et al.*, "Potential of subdermal solar energy harvesting for medical device applications based on worldwide meteorological data," *J. Biomed. Opt.*, vol. 26, no. 3, Mar. 2021, Art. no. 038002.

[11] K. Goto *et al.*, "An implantable power supply with an optically rechargeable lithium battery," *IEEE Trans. Biomed. Eng.*, vol. 48, no. 7, pp. 830–833, Jul. 2001.

[12] S. Ayazian *et al.*, "A photovoltaic-driven and energy-autonomous CMOS implantable sensor," *IEEE Trans. Biomed. Circuits Syst.*, vol. 6, no. 4, pp. 336–343, Aug. 2012.

[13] E. Moon, D. Blaauw, and J. D. Phillips, "Subcutaneous photovoltaic infrared energy harvesting for bio-implantable devices," *IEEE Trans. Electron Devices*, vol. 64, no. 5, pp. 2432–2437, May 2017.

[14] T. Wu, J.-M. Redoute, and M. R. Yuce, "A wireless implantable sensor design with subcutaneous energy harvesting for long-term IoT healthcare applications," *IEEE Access*, vol. 6, pp. 35801–35808, Jul. 2018.

[15] K. Song *et al.*, "Subdermal flexible solar cell arrays for powering medical electronic implants," *Adv. Healthcare Mater.*, vol. 5, pp. 1572–1580, May 2016.

[16] J. Kim *et al.*, "Active photonic wireless power transfer into live tissues," *Proc. Nat. Acad. Sci.*, vol. 117, pp. 16856–16863, Jul. 2020.

[17] A. Haeberlin *et al.*, "Successful pacing using a batteryless sunlight-powered pacemaker," *EP Europace*, vol. 16, pp. 1534–1539, Jun. 2014.

[18] A. Haeberlin *et al.*, "The first batteryless, solar-powered cardiac pacemaker," *Heart Rhythm*, vol. 12, pp. 1317–1323, Jun. 2015.

[19] V. Guiheneuf, F. Delaleux, S. Pouliquen, O. Riou, P.-O. Logerais, and J.-F. Durastanti, "Effects of the irradiance intensity during UV accelerated aging test on unencapsulated silicon solar cells," *Sol. Energy*, vol. 157, pp. 477–485, Nov. 2017.

[20] N. Franzina *et al.*, "A miniaturized endocardial electromagnetic energy harvester for leadless cardiac pacemakers," *Plos One*, vol. 15, Sep. 2020, Art. no. e0239667.

[21] Wacker, ELASTOSIL RT 601 A/B. Wacker Chemie AG, Jul. 2020. Datasheet.

[22] YOLK, YOLK High Efficiency Solar Modules - YKSM 4-4-0.5-5. Yolk, 655 W. Irving Park Rd, 4302 Chicago, IL 60613, United States, 2017. *Datasheet*.

[23] AMS, ASM AS7265x. AMS AG, Tobelbader Strasse 30, 8141 Premstaetten, Austria, v 1–04 ed., Jul. 2018. *Datasheet*.

[24] ASM AS7341 AMS. AMS AG, *Tobelbader Strasse* 30, 8141 Premstaetten, Austria, v 1–04 ed., Oct. 2018. Datasheet.

[25] O. Optics, USB4000 Data Sheet. *Ocean Optics*, 830 Douglas Ave., Dunedin, FL 34698, United States. Datasheet.

[26] S. A. Ranamukhaarachchi *et al.*, "A micromechanical comparison of human and porcine skin before and after preservation by freezing for medical device development," *Sci. Rep.*, vol. 6, no. 1, pp. 1–9, Aug. 2016.

[27] N. Voudoukis and S. Oikonomidis, "Inverse square law for light and radiation: A unifying educational approach," *Eur. J. Eng. Res. Sci.*, vol. 2, pp. 23–27, Nov. 2017.

[28] C. Hillard *et al.*, "Silicone breast implant rupture: A review," *Gland Surg.*, vol. 6, pp. 163–168, Apr. 2017.

[29] TI, bq25570 Nano Power Boost Charger and Buck Converterfor Energy Harvester Powered Applications. Texas Instruments Incorporated, 12500 TI Boulevard, Dallas, TX 75243, USA, slusbh2g ed., Mar. 2019. Datasheet.

[30] S. L. Jacques, "Optical properties of biological tissues: A review," *Phys. Med. Biol.*, vol. 58, pp. R37–R61, May 2013.

[31] N. Bosschaart *et al.*, "A literature review and novel theoretical approach on the optical properties of whole blood," *Lasers Med. Sci.*, vol. 29, pp. 453–479, Oct. 2013.

[32] G. Yoon *et al.*, "Development and application of three-dimensional light distribution model for laser irradiated tissue," *IEEE J. Quantum Electron.*, vol. 23, no. 10, pp. 1721–1733, Oct. 1987.

[33] R. L. van Veen *et al.*, "Determination of VIS- NIR absorption coefficients of mammalian fat, with time- and spatially resolved diffuse reflectance and transmission spectroscopy," in *Proc. Biomed. Top. Meeting*, 2004, Paper SF4.

[34] R. Klopfleisch and F. Jung, "The pathology of the foreign body reaction against biomaterials," *J. Biomed. Mater. Res. Part A*, vol. 105, pp. 927–940, Nov. 2016.

[35] H. Patel and V. Agarwal, "MATLAB-based modeling to study the effects of partial shading on PV array characteristics," *IEEE Trans. Energy Convers.*, vol. 23, no. 1, pp. 302–310, Mar. 2008.

[36] A. Bidram, A. Davoudi, and R. S. Balog, "Control and circuit techniques to mitigate partial shading effects in photovoltaic arrays," *IEEE J. Photovolt.*, vol. 2, no. 4, pp. 532–546, Oct. 2012.

[37] O. Bingöl and B. Özkaya, "Analysis and comparison of different PV array configurations under partial shading conditions," *Sol. Energy*, vol. 160, pp. 336–343, Jan. 2018.

[38] M. C. Y. Heng, "Wound healing in adult skin: Aiming for perfect regeneration," *Int. J. Dermatol.*, vol. 50, pp. 1058–1066, Aug. 2011.

[39] S. K. V. Sekar *et al.*, "Diffuse optical characterization of collagen absorption from 500 to 1700 nm," *J. Biomed. Opt.*, vol. 22, Jan. 2017, Art. no. 015006.

[40] L. Bereuter *et al.*, "Energy harvesting by subcutaneous solar cells: A long-term study on achievable energy output," *Ann. Biomed. Eng.*, vol. 45, pp. 1172–1180, Jan. 2017.